Journal of Sedimentary Research

Journal of Sedimentary Research, 2019, v. 89, 28–45
Research Article
DOI: http://dx.doi.org/10.2110/jsr.2019.2

LATERAL FACIES VARIABILITY ALONG THE MARGIN OF AN OUTCROPPING SALT-WITHDRAWAL MINIBASIN, SOUTH AUSTRALIA

JOHN W. COUNTS,[1,3] CHARLES R. DALGARNO,[2] KATHRYN J. AMOS,[3] AND STEPHEN T. HASIOTIS[4]
[1]*Irish Centre for Research in Applied Geosciences (iCRAG), O'Brien Centre for Science, University College Dublin, Belfield, Dublin 4, Ireland*
[2]*20 Hedley Street, Mt. Gambier, South Australia 5290, Australia*
[3]*Australian School of Petroleum, Level 2 Santos Petroleum Engineering Building, University of Adelaide, Adelaide, South Australia 5005, Australia*
[4]*University of Kansas, Department of Geology, 1475 Jayhawk Boulevard, 120 Lindley Hall, Lawrence, Kansas 66045, U.S.A.*
e-mail: jwcounts@gmail.com

ABSTRACT: **Many aspects of depositional processes adjacent to exposed evaporite diapirs are not well understood, yet these processes are key to understanding sediments that are part of economically important hydrocarbon systems around the world. In the Adelaide Rift Complex of South Australia, diapirs intersected the seafloor and land surface during the Ediacaran–Cambrian at the same time as sediment was being deposited. Excellent exposures of these diapirs and their associated minibasins allow the character and distribution of these deposits to be studied in detail; this study examines the interaction between a diapir body and minibasin sediments from a sedimentological perspective. Numerous sections were measured along the minibasin margin, allowing the sedimentary facies, lateral sediment variability, and depositional processes to be determined. Deposition took place in a variety of environments, ranging from carbonate shelves to subaerially exposed tidal flats and alluvial fans. Minibasin sedimentation adjacent to the diapir is characterized by an abundance of gravity-flow deposits, including turbidites and debrites. These deposits often contain extraformational conglomerates brought to the surface by the diapir and redeposited into the minibasin depocenter. Within the minibasin fill, sedimentary facies are unevenly distributed, and sedimentary character is most affected by the diapir in areas where depositional thinning, onlap, and growth faulting are most common. Comparison of our observations with other localities where salt bodies intersect the surface show that syndepositional salt–sediment interaction results in a recurring set of features that can be useful in predicting the sedimentary character of these deposits. This study is one of relatively few to examine the sedimentology of an outcropping minibasin in detail and to describe lateral variability of sedimentary facies along an outcropping minibasin margin. The deposits discussed here therefore provide a valuable analogue for subsurface and seafloor deposits elsewhere where salt–sediment interactions cannot be studied in detail.**

INTRODUCTION

Salt-tectonic deformation affects over 120 basins around the world, including some of the world's largest petroleum-producing fields, yet most of these provinces occur only in the subsurface or on deepwater continental margins (Hudec and Jackson 2007). Among those visible at the surface, many are inaccessible due to a lack of well-exposed surficial geology, remote outcrop locations, or geopolitics, and many outcrop studies focus primarily on structural aspects of diapir emplacement and the reconstruction of halokinetic sequences (e.g., Giles and Lawton 2002; Backé et al. 2010; Hearon et al. 2015a). Although several recent studies have examined salt-withdrawal minibasins from a sedimentological perspective (e.g., Aschoff and Giles 2005; Matthews et al. 2007; Kernen et al. 2012; Banham and Mountney 2013a, 2013b, 2014; Ribes et al. 2015; Counts and Amos 2016), more research is needed to fully characterize these unique depositional settings. The purpose of this study is to describe and interpret salt–sediment interaction and lateral facies change along the obliquely exposed margin of an Ediacaran salt-withdrawal minibasin from South Australia, creating an outcrop analogue that can be used to better understand similar deposits in more inaccessible settings. This is accomplished through detailed geological mapping and the measurement of eight stratigraphic sections from the diapir contact into the minibasin interior.

Subsidence of sedimentary strata due to the mobilization of underlying evaporites often results in the formation of small basins at a scale of tens of kilometers (Hudec and Jackson 2006; Peel 2014). These minibasins (rim synclines) are often important elements of hydrocarbon systems, forming topographic lows and depocenters on the seafloor or land surface (Bryant et al. 1990; Booth et al. 2003) that can affect reservoir quality and create structural and stratigraphic traps (Toniolo et al. 2006; Pilcher et al. 2011). In the study area described here, minibasin deposits are exposed at the surface in oblique map view, permitting continuous observations along the eastern flank of the diapir and the minibasin. Exposed strata display multiple indications of interaction between sediments and the diapir itself, which resulted in erosional surfaces and unique facies not present in these formations away from the influence of the diapir. As such, the results shown here provide a unique record of the direct effects of diapir exposure on sedimentology and stratigraphy. These findings will prove useful for the interpretation of analogous systems elsewhere, as this paper is one of only

Published Online: January 2019
 1527-1404/19/089-028

a relatively few published outcrop studies to document kilometer-scale spatial changes in minibasin facies. The findings from this type of study (e.g., the lateral changes in lithologies, depositional processes, and stacking patterns that result from the proximity to an exposed diapir) can be applied elsewhere in order to add to our understanding of the environments, processes, and architectural elements of minibasin fill, all of which have economic importance in the oil and gas industry. Given that such studies remain relatively rare, an opportunity exists for much more work to be done on the sedimentology of systems influenced by salt tectonics. Ultimately, the interpretation of minibasins may benefit from a facies-models approach, in much the same way that other depositional environments have (e.g., Posamentier and Walker 2006). The investigation presented here is another step toward an improved understanding of the depositional processes and products associated with salt–sediment interaction.

In this study, we aim to (1) document minibasin sediments and how they differ in the Mt. Frome minibasin from the sediments located elsewhere in the basin; (2) interpret the depositional environments and geomorphologic features present in the minibasin; and (3) determine the ways that salt movement and proximity to an exposed diapir body affected depositional processes in the study area.

GEOLOGIC SETTING

Tectonic Background of the Adelaide Rift Complex

The minibasin deposits discussed here are present in the Adelaide Rift Complex (ARC), a north–south-trending basin now partially exposed in the Ikara–Flinders Ranges of South Australia (Fig. 1). Beginning as a tripartite aulacogen, basin sedimentation began during the breakup of Rodinia around 800 Ma (Preiss 1987; Bogdanova et al. 2009). Infilling of the basin continued until the Cambrian, as the basin gradually evolved from a restricted rift into a passive margin (Preiss 1987, 2000). This resulted in a thick sedimentary fill that was significantly affected by contemporaneous diapir movement and sedimentation. Evaporites in the basin fill were likely the product of restriction during the initial period of rifting, although the autochthonous level is rarely exposed in its original stratigraphic position (Hearon et al. 2015a, 2015b) and much information about the origin and nature of evaporite deposition remains enigmatic (Backé et al. 2010). Salt mobilization began early in the basin's history, as many older Neoproterozoic deposits show interaction with diapirs (Dyson 2004b), and continued at least until the early Cambrian (Dalgarno and Johnson 1968; Reilly 2001). By Ediacaran time, the ARC formed part of an Australia–East Antarctica subcontinent, which was likely in low latitudes just north of the equator (Li et al. 2008). The southern end of the basin is inferred to have been an oceanic connection, and the northern extent may also have been a deeper-water depocenter (Preiss 1987; Counts and Amos 2016). A compressional episode, the Delamerian Orogeny, deformed basin sediments in the mid Cambrian and shortened the basin in an east–west direction by as much as 10–20% (Paul et al. 1999). This event, combined with more recent intra-plate uplift and a modern arid climate, has resulted in excellent exposures of the basin fill, including minibasin deposits.

Background Sedimentation

In order to assess the effects of syndepositional diapirism, the typical "background" lithologies and depositional environments in the stratigraphic interval of interest outside the minibasin must first be understood. These are summarized in Table 1, and belong to the Wilpena Group (Brachina and Wonoka formations, Bonney Sandstone, Rawnsley Quartzite) and Hawker Group. Elsewhere in the basin, these formations are usually separated by unconformities, and span approximately 40 million years of deposition (Preiss 2000). The base of the Wilpena Group (Mawson 1941), marks the Global Stratotype Section and Point (GSSP) for base of the Ediacaran Period, between 600 and 635 Ma (Knoll et al. 2006). The Wilpena Group, the focus of this study, comprises two large-scale, shallowing-upward sequences that terminate at the Cambrian boundary. In the lower Cambrian (Terreneuvian), much of the basin was blanketed by a fine-grained carbonate ramp (Hawker Group), deepening to the north with a variety of microbial, sponge, and archaeocyathid reef buildups (Dalgarno 1964; James and Gravestock 1990).

Character and Distribution of Diapirs in the Adelaide Rift Complex

Throughout much of its history, basin topography may have resembled modern-day, salt-influenced provinces similar to those seen in the Barents Sea and elsewhere. Indeed, much of the current structural complexity in the basin likely predates the Delamerian Orogeny and is likely the product of salt tectonics (Rowan and Vendeville 2006). The Delamerian Orogeny exaggerated existing synforms and antiforms, reactivated and reversed growth faults, and tilted strata such that diapirs and their adjacent minibasins are presently oriented in plan, cross-sectional, and/or oblique views. When exposed, diapirs are most often found today as kilometer-scale, irregular-shaped bodies that are isolated from one another by tens of kilometers, though they may be connected by faults or salt welds. Specific locations where diapir mobilization occurred were likely controlled by pre-existing basement faults (Backé et al. 2010).

A lack of subsurface data (e.g., well logs, core, seismic) in the Ikara–Flinders Ranges prevents complete characterization of the distribution and three-dimensional (3D) morphology of salt bodies. Where visible in cross section, some diapirs connect autochthonous salt to allochthonous, stratigraphically higher salt bodies. Diapirs appear to have broken out and flowed along bedding planes (Dyson 2004a; Hearon et al. 2015a). The effects of salt withdrawal are evident in strata throughout the basin, with minibasins of various scales occurring adjacent to many exposed diapirs. Minibasins are often asymmetric, indicating differential subsidence across their axes, and are occasionally bounded by welds where salt has moved upward and been evacuated from the minibasin margin. Asymmetry in stratal thickness is also present on either side of diapirs themselves, a result of the changing locus of minibasin subsidence over time.

Present-day diapirs exposed at the surface do not contain any remaining evaporite minerals; current exposures consist of a mixed-lithology breccia with a microcrystalline dolomitic matrix (Fig. 2A, B; Preiss 1987). The current diapir expression is often interpreted as a caprock, formed when the evaporite matrix of the diapir is dissolved or replaced by carbonate (Dyson 2004a). The high density of clasts seen is the result of the concentration of associated sediments left behind during weathering of more soluble material (Cooper 1991). Clasts in this matrix are highly angular, ranging in size from pebbles to kilometer-scale blocks (Fig. 2C, D), and are composed of a wide variety of lithologies. Observed rock types include consolidated, bedded, often fine-grained clasts of sedimentary rocks, basalts, and other fine-grained mafic volcanics. These lithologies are interpreted as originating from Callanna Group strata that were interlayered with evaporites at the time of deposition and were entrained into the plastically flowing diapir as it moved upward (Dalgarno and Johnson 1968).

METHODOLOGY

The focus of this study is an asymmetric minibasin near the eastern margin of the ARC, the Mt. Frome minibasin and diapir (Fig. 3A, B). Features of interest were identified from regional geologic maps (Reid and Preiss 1999) and reconnaissance field trips. Geographically, the study area is on the eastern margin of the central Ikara–Flinders Ranges, approximately 50 kilometers east of the town of Blinman. The arid climate in the region permits excellent exposures of the underlying geology

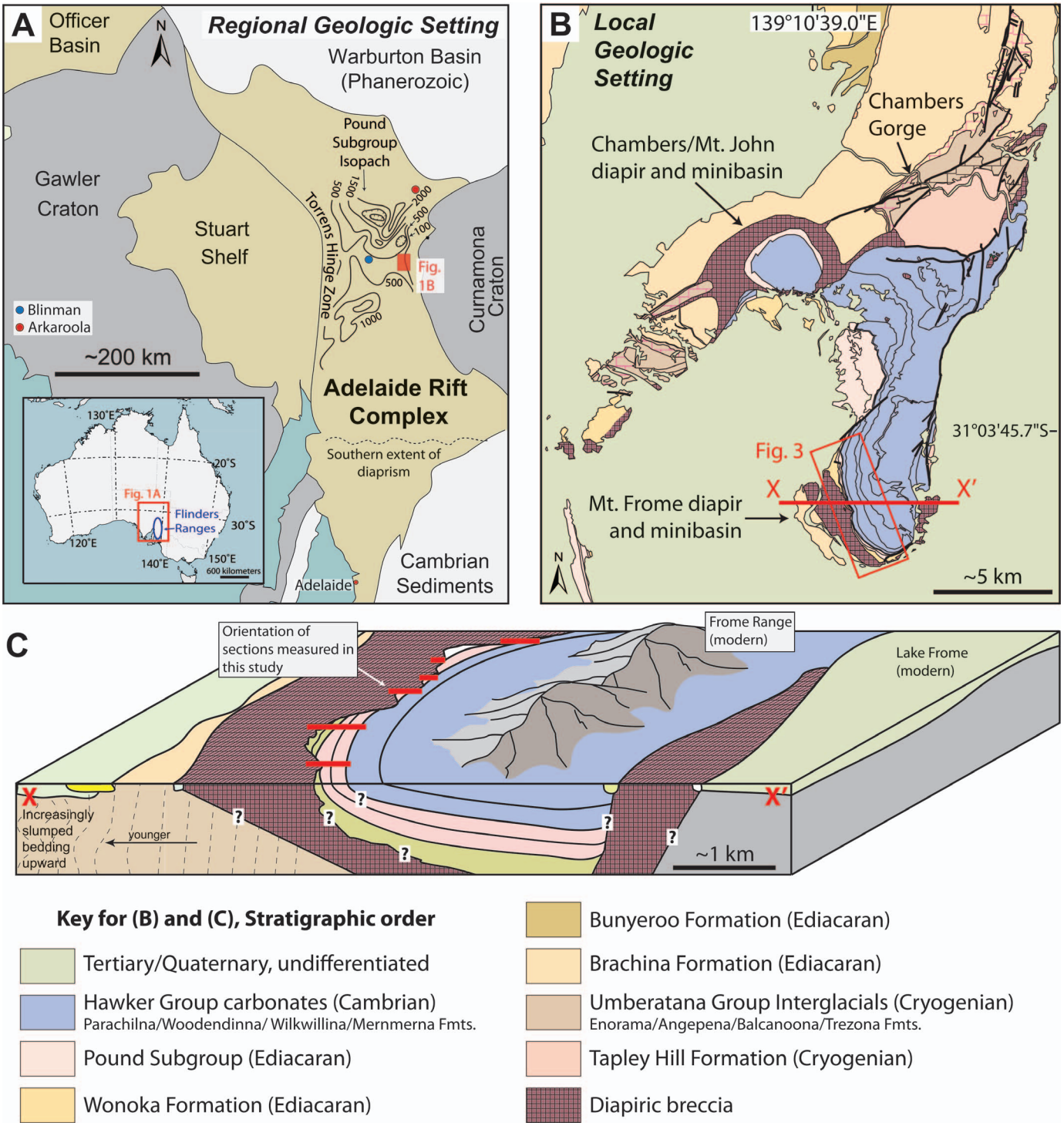

FIG. 1.—Location and geologic context of study area. **A)** Location of Ikara–Flinders Ranges and Adelaide Rift Complex in Australia. Red square in inset marks location of enlarged map in Figure 1, Part B. **B)** Portion of Geological Survey of South Australia geologic map (Preiss 1999) of the Mt. Frome region. Red square marks location of Figure 3A. Pound Subgroup isopach from Gehling (1982). **C)** 3-D block showing schematic cross-section across the minibasin from X to X′ in above map, and inferred orientation of strata examined in this study. Map and cross-sectional views, and placement of measured sections, are schematic only; see Figure 3 for actual geologic map. Much of the subsurface geology is inferred due to lack of data.

due to the lack of vegetation and soil cover; however, exposure is not completely continuous as thin calcarosols (McKenzie et al. 2004), Pleistocene outwash terraces, and Quaternary alluvium intermittently cover the region.

For this study, eight stratigraphic sections were measured, spanning a five-kilometer transect along the diapir–sediment contact (Fig. 3A). Lithostratigraphic contacts and faults were mapped along the transect in substantially more detail than the original 1:250,000-scale geologic map,

TABLE 1.—Summary of typical lithologies of formations in this study, for comparison with diapir-influenced character in the Mt. Frome region.

Unit		Summary Description	Interpretation	Primary Reference
Hawker Group		Wilkawillina Formation: 230 m-thick, three members, generally massive, gray, clean lime mudstone and wackestone, elsewhere with archaeocyath–*Renalcis* bioherms and shelly fossils	Carbonate ramp blanketing most of the basin. Occasional structurally controlled bioherms with associated lagoons and subaerial exposure surfaces.	Dalgarno 1964
		Probable unconformity, with lowermost Cambrian Formations not present. Hawker Group carbonates (above) likely part of Wilkawillina Limestone.		
Wilpena Group	Rawnsley Quartzite	400 m thick, three members; the lowermost Chace Member consists of clean, algal-laminated quartzites, separated from above units by a deep incision surface. The Ediacara Member is characterized by cross-stratified channelized sands and thin beds of siltstones, among other facies. It hosts the well-known "Ediacaran fauna," and is overlain by a thick, unnamed unit of clean sandstones similar to that seen at the base.	Intertidal sand flat and sabkha in the Chace Member, with a relative sea-level fall in the Ediacara Member incising-valleys and depositing shallow marine clastics as incised valley fill, including prodeltaic silts, mass-flow fluidized channels, and storm-dominated delta-front sands. The upper member is primarily composed of thick wave- and tide-influenced shallow marine delta sands.	Gehling 1982; Gehling 2000
	Bonney Sandstone	~ 300 m thick in the type section; two members: the lower Patsy Hill Member and an upper unnamed member. The Patsy Hill Member was traditionally included in the Wonoka Formation and was revised to the Bonney Sandstone in 1999. The Patsy Hill Member consists of limestone–sandstone parasequences with algal and stromatolitic features in carbonates and red, micaceous sandstones. Upper member consists of several coarsening-upward parasequences of reddish siltstones and sandstones.	Patsy Hill Member: shallow marine to lagoonal stormy carbonate ramp, shallowing up to ooid shoals and hardgrounds, with clastics being subtidal or intertidal. In the upper Bonney, fluvial–deltaic sands prograding onto a fine-grained shelf, forming a highstand systems tract with sands originating from the Musgrave Province to the north.	Haines 1990; Counts 2016; Counts et al. 2016
	Wonoka Formation	700 m thick; basal Wearing Dolomite Member contains shale and dolomicrite. Divided originally into 12 units containing calcareous siltstones, silty limestones, and red and green siltstones and mudstones. Major unconformity in upper part of formation marked by kilometer-deep canyons that incise into the Bunyeroo Formation.	Storm-dominated carbonate ramp/shelf, overlain by marine canyon fill and lagoonal and intertidal carbonates. Deepens substantially to the north with interspersed diapiric islands.	Haines 1990
		ABC Range Sandstone, Wilcolo, and Bunyeroo Formations not present in immediate study area.		
	Brachina Formation	1250 m thick, three members; Red-brown and olive green siltstones and shale, sometimes cyclically interbedded with cross-stratified sandstones, gradational upper contact with ABC Range Sandstone	Generally very low energy, subtidal clastic shelf conditions, progressively shallowing upward to progradational deltaic sands from the Gawler Craton	Leeson 1970; Plummer 1978; Preiss et al. 1993

and field observations were later combined with high-resolution aerial photos to produce the detailed map in Figure 3A. Relatively continuous sections of bedrock are exposed along stream cuts and hilltops at certain points along the transect, permitting measurement of stratigraphic sections. Unit thicknesses were determined using tape measure and GPS (generally ± 2–4 m accuracy), incorporating structural dip to attain true stratigraphic thickness. Paleocurrent readings were taken where such sedimentary structures as ripples, cross-stratification, or channels were clear enough to permit unambiguous data collection. Two directions were recorded for symmetrical ripples and other bidirectional features; crest orientation was recorded for wave ripples on rose diagrams. Structural tilt was removed at the time of measurement. These data were used to assess the orientation of the paleoshoreline and the dominant flow direction of unidirectional currents in the minibasin.

OBSERVATIONS

The Mt. Frome minibasin discussed here (Figs. 1, 3) is partially upturned and exposed in an oblique cross-sectional view, revealing both lateral and stratigraphic changes in sedimentary facies around minibasin margins. Although the specific exposure orientation and three-dimensional geometry of the minibasin cannot be determined with certainty, the exposures seen here provide enough information to assess the lateral variability of minibasin sediments across several kilometers. The transect traverses the margin of the diapir body, with the contact between the diapir and adjacent sediments intermittently exposed. In general, structural dips of sediments are steepest near the diapir margin (sometimes approaching 90°) and decrease into the basin to the east (selected measurements in Fig. 3A) with Cambrian deposits having the shallowest dips. Dip magnitude, however, is locally variable. Diapir-involved faulting is also common along the margin. A closely spaced series of normal faults near the center of the transect downdrop both the diapir and minibasin deposits to the south. These deposits show lithological and thickness changes across the faults. Barite veins and mineralized, brecciated zones are also present in this area. Faults also occur to the north and south of this central area, but are more spread out, and without consistent orientations (Fig. 3).

Facies Descriptions

Observations from the measured sections are presented in Figures 4–6 and Table 2. Eight facies (Figs. 6, 7) were observed in the minibasin fill, distinguished by a particular combination of lithologies and sedimentary structures (examples shown in Fig. 8). Mapped formations consist of one or more facies; contacts between these are usually sharp. Paleocurrents measured on symmetrical and asymmetrical ripples were most frequently taken in Facies D and E, shown in Figure 5; asymmetric ripples show an eastward-dominated flow direction. Symmetrical ripple marks (crest orientations shown in Fig. 5) indicate a generally north–south-trending shoreline, aside from a single opposing measurement. There was no obvious spatial trend in paleocurrent orientation.

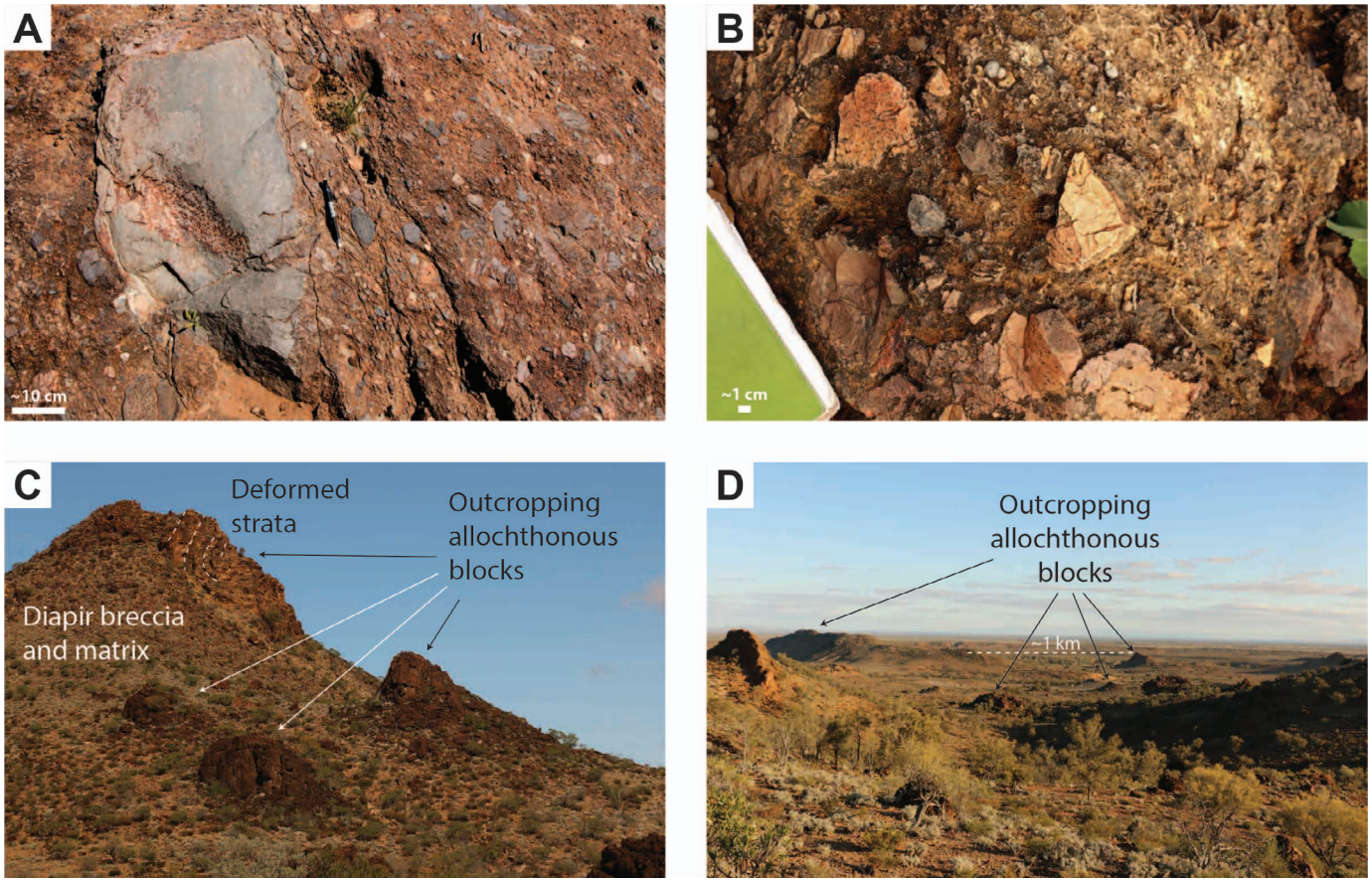

FIG. 2.—Diapir lithologies and outcrops. **A**, **B)** Typical diapir lithologies in the study area, consisting of large angular rock fragments in a fine-grained dolomitic matrix. **C**, **D)** Outcrop expressions of the Mt. Frome diapir, showing kilometer-scale allochthonous blocks entrained in diapir matrix.

Facies Distribution

Facies are generally stacked atop one another and rarely repeated stratigraphically upward (Fig. 6). Contacts between formations coincide with some facies boundaries (e.g., Facies C to D and E to F) and are often sharp, suggesting that they are unconformable. Within formations, vertical facies transitions are also usually abrupt, with new lithologies (i.e., gravel beds) appearing suddenly. Laterally, facies are unevenly distributed across the study area. Facies A (red calcareous shale and limestone; Fig. 7A) occurs only at the base of the Wonoka Formation in the northern part of the study area near measured sections 1 and 2, and thins out southward to zero from a maximum observed thickness of $\sim$ 100 m over the course of $\sim$ 1.75 km. Facies B and C (yellow shales, also in the Wonoka Formation, with and without clastic pebbles, respectively; Fig. 7B, C) are present in both the northern and southern parts of the minibasin, but they onlap an apparent diapir high in the center of the transect, and are not present in measured sections 3–5 (Figs. 3, 4). Facies C is present as a distinct unit within or near the top of Facies B, and the two facies together have a maximum thickness of $\sim$ 200 m on the northern end (section 1). Together, both facies thin southward until they terminate into a fault between sections 2 and 3, about 2 km from their northernmost exposure. On the southern end of the minibasin, these facies reach $\sim$ 140 m in thickness (section 7) and thin out to the north over the course of $\sim$ 1.5 km. Red sandstones and shales of Facies D (Fig. 7D) also occur in the northern and southern sections; however, this facies transitions laterally into Facies E rather than onlapping onto the central part of the diapir. Pebble–cobble-dominated sediments of Facies E (Fig. 7E) are present predominantly in the central portion of the transect, where they are the only Precambrian strata present. Taken together, Facies C and D therefore thin centrally, from a maximum of $\sim$ 130 m in section 7 to about 55 m at minimum in section 4 (Fig. 6). Facies E often takes the form of lens-shaped beds of conglomerates and sands, with conglomerate clasts sometimes (though rarely) containing casts of cubic halite crystals. Conglomerates in these beds may be capped by fining-upward sands, but more commonly are unsorted and in sharp contact with overlying and underlying sandy shales. These discontinuous beds range in scale from meters to tens of meters laterally, and are generally $<$ 1 m thick. Facies F (Fig. 7F) occurs in the Bonney Sandstone as a discrete, sharp-based unit that is tens of meters thick and incises into the typical sand–shale Bonney Sandstone lithologies (Facies D) in the northern part of the study area. The unit is traceable in aerial photos across hundreds of meters, and can be seen to truncate beds lower in the section (dashed orange line, Fig. 3A). Clean, white sandstones of Facies F also occur in the unit overlying the Bonney Sandstone—the Rawnsley Quartzite—in southern measured sections 5–7, although there it is more dominated by irregularly laminated sands. Recent sedimentary cover on the northern and southern ends of the transect obscures further

→

FIG. 3.—**A)** Detailed geologic map of the minibasin and diapir that are the focus of this study, and locations of sections shown in Figures 4 and 6. Bases of sections always to the south or southwest. **B)** Detail of central part of minibasin, showing irregular minibasin margin and faulting.

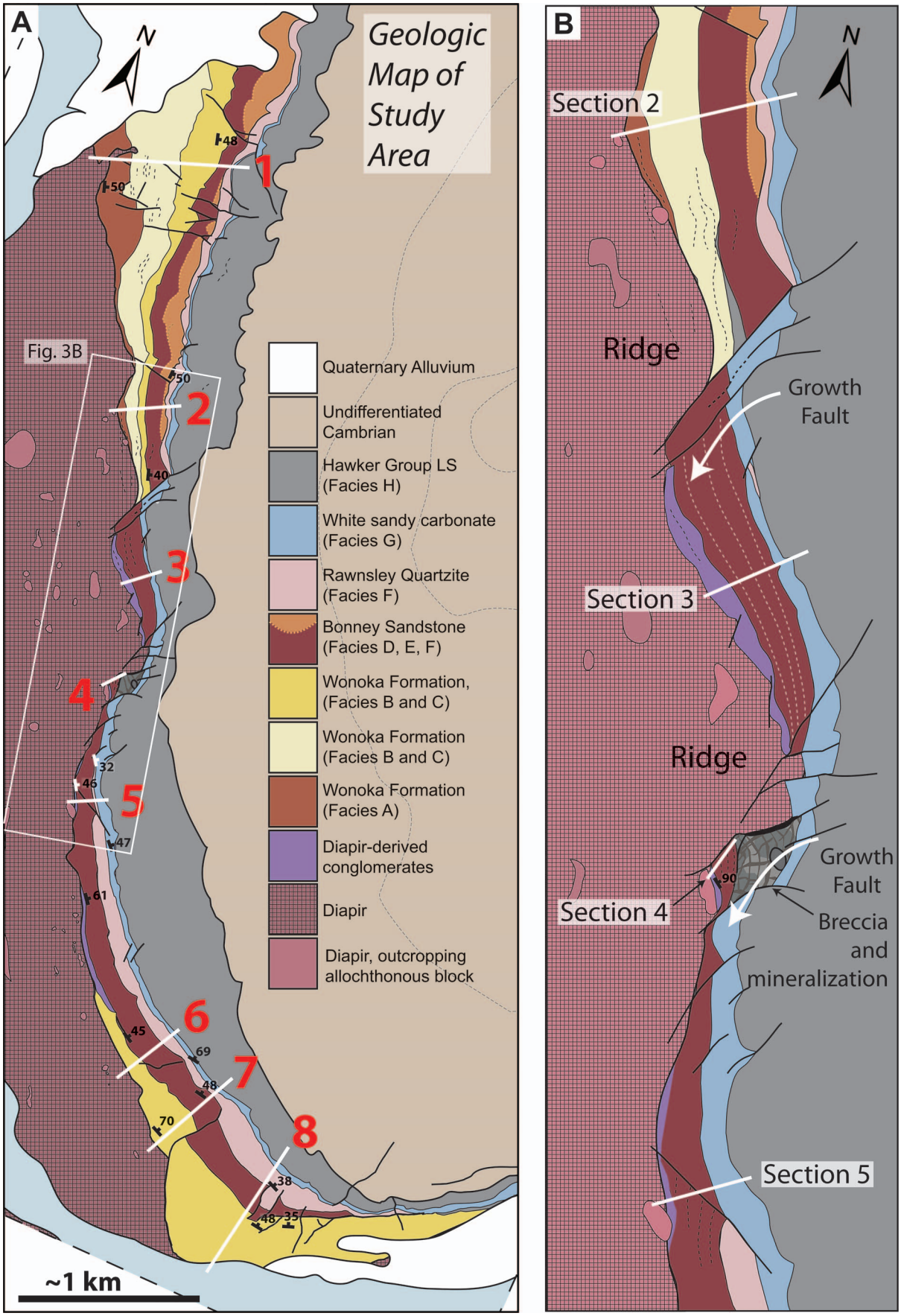

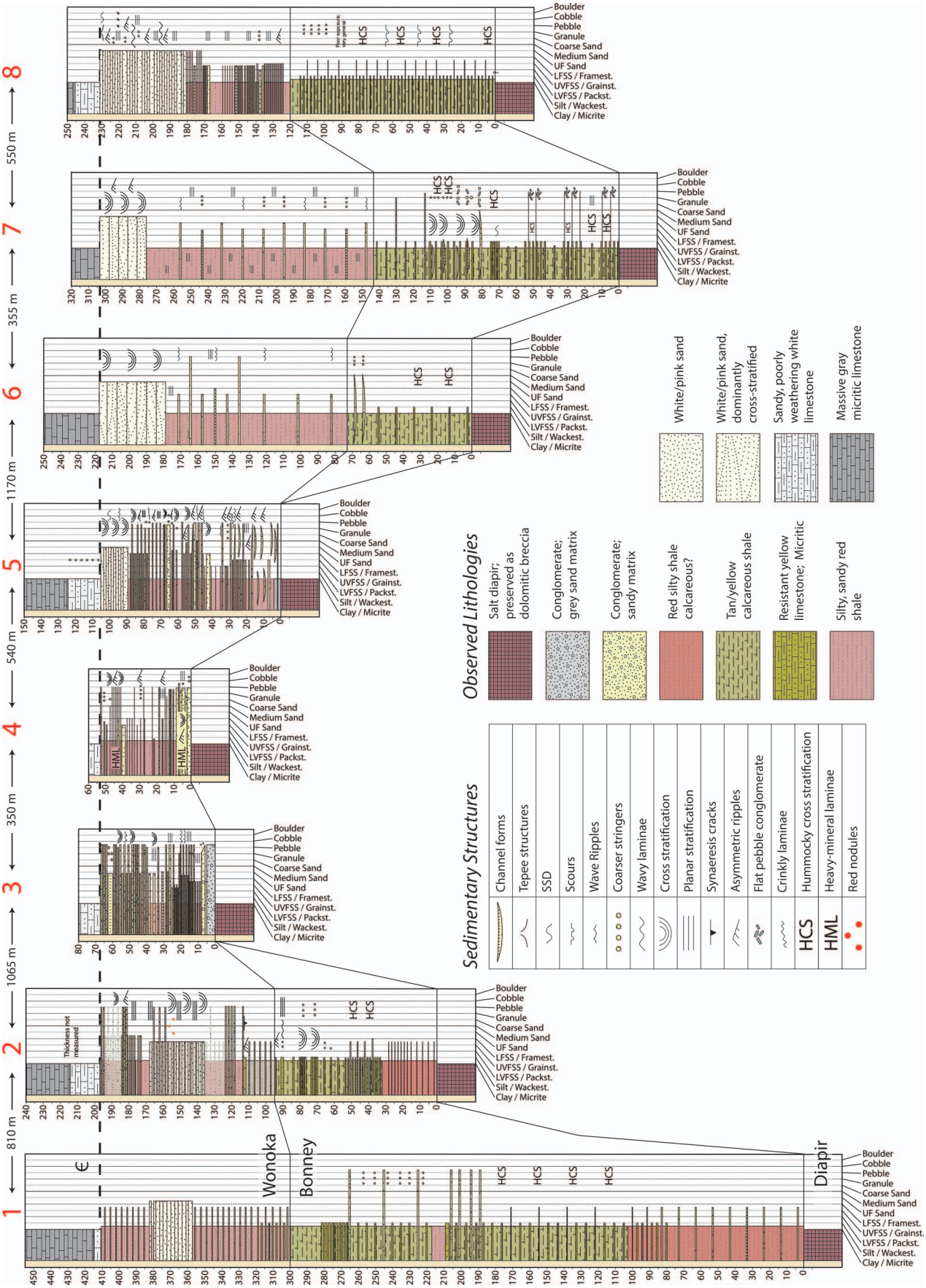

FIG. 4.—Stratigraphic sections measured in this study, with thickness values in meters. Datum is base of Cambrian limestones. Locations shown in Figure 3; waypoints in JSR's Data Archive (see Supplemental Material).

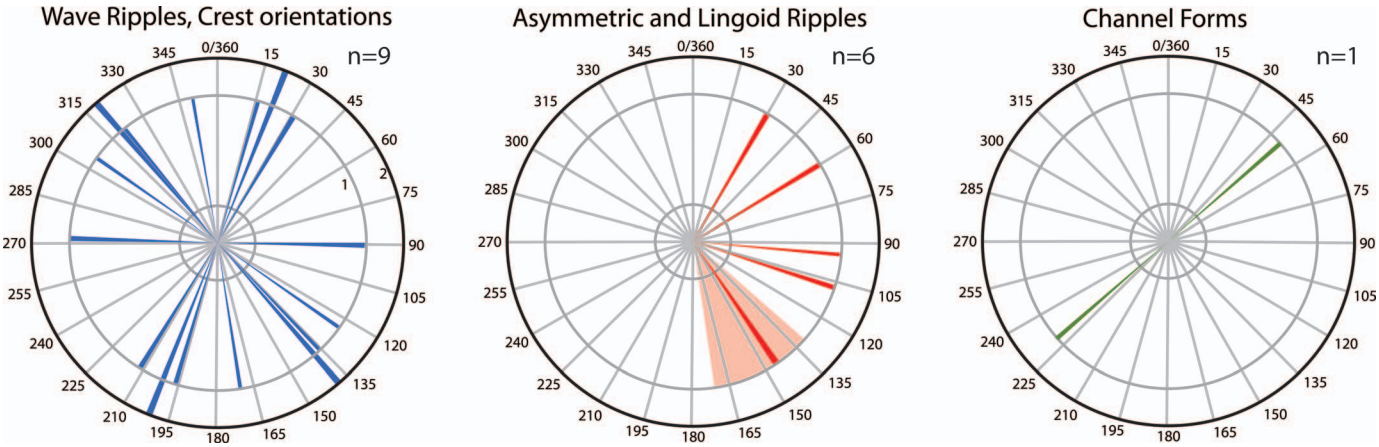

FIG. 5.—Combined paleocurrent data from all sections. For wave (symmetrical) ripples, crest orientations are shown.

relationships. The transgression of early Cambrian carbonates (Facies G, Fig. 7G) is persistent across the minibasin. Hawker Group micritic carbonates (Facies H, Fig. 7H) blanket the minibasin at the top of the sections measured, and are generally lithologically consistent throughout.

Facies Interpretations

Fine-grained carbonates of Facies A and B are interpreted to be relatively similar in their environments of deposition, likely on a carbonate ramp or shelf. The common presence of hummocky cross-stratification (HCS) intermittently interspersed between thicker intervals of lower-energy sedimentation suggests that the area was periodically affected by storms that caused reworking of cleaner (i.e., less clastic shale content), shallow-water carbonates into the deeper parts of the basin (Haines 1988). The lack of wave ripples in these facies indicates they were below fairweather wave base and above storm wave base. Red coloration in the Wonoka Formation, similar to that in Facies A, has previously been interpreted as the product of increased oxygenation of the water, related to "deep shelf currents below a stagnant middle shelf zone" (Haines 1990), though recent studies on adjacent formations (Tarhan et al. 2017) suggest that red color is a recent diagenetic phenomenon. Flat pebble clasts in these facies are all composed of carbonate, and are thought to have originated nearby as rip-up clasts during storm conditions.

Facies C marks the earliest stratigraphic occurrence of clastic grains in the section, in the form of clastic pebble beds, although background lithologies and interpretations are similar to those above for Facies A and B, which lack clastic pebbles. Pebble beds (Fig. 8A, B) are often seen in association with cleaner, HCS limestones, which suggests that they, too, may be related to storm events. Clasts in these beds are similar in composition, though more rounded, to those seen in the diapir matrix itself. Clast are composed primarily of lithified sediments, including fine-grained mudstones, silts, and fine-grained sands with ripple cross-stratification preserved in cross section, as well as quartz pebbles and rare cobble-size shale clasts with apparent halite pseudomorphs. Accumulations of pebble-size clastic debris are not found elsewhere in the Wonoka Formation, except for where they have been reported near other diapirs (Haines 1987; Kernen et al. 2012; Hearon et al. 2015a), providing a clue to their origin. These beds and the clasts within them are interpreted to originate from the

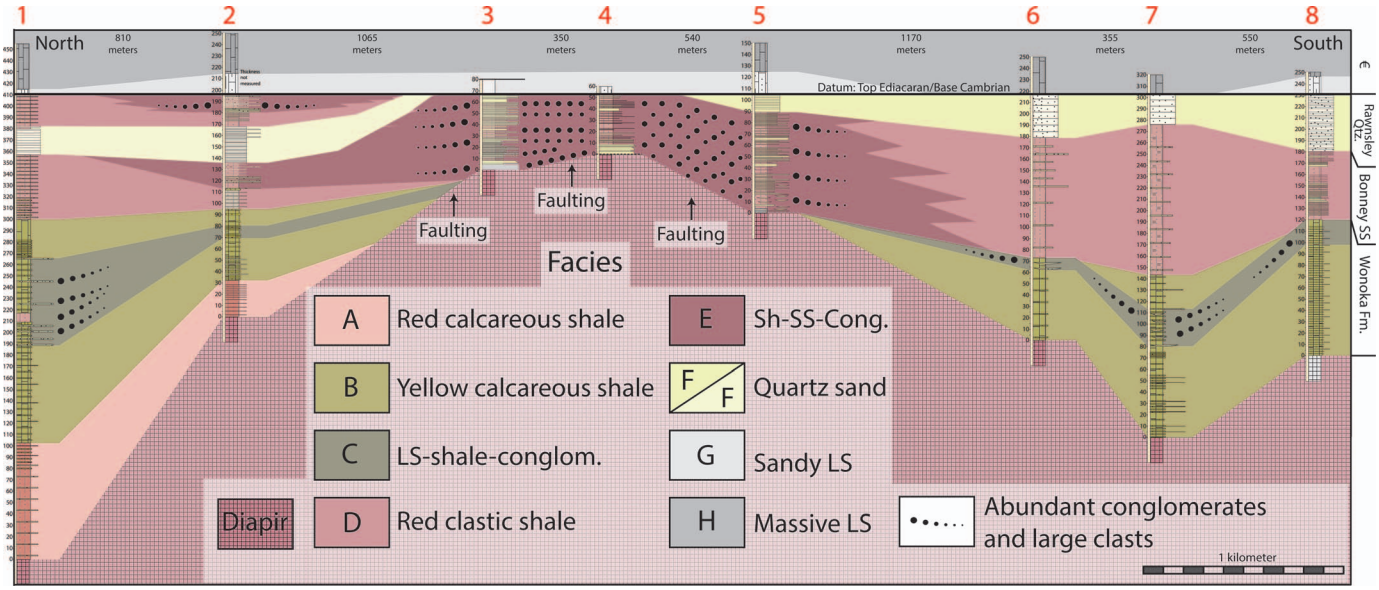

FIG. 6.—Facies relationship diagram for the Mt. Frome minibasin margin. Labeled sections correspond to those in Figure 3. Diagram is schematic and does not show the complexities of facies change between sections.

TABLE 2.—Summary of sedimentary facies in the minibasin, and schematic representation of each facies in cross section. Each drawing is intended to represent 1–2 meters of section. Colors are representative of sediment color, and lithologic patterns correspond to those in Figure 6. Facies G not shown due to poor exposure.

Age	Unit	Facies Name	Diapir-derived material?	Description	Environments/ Processes	Figure
Cambrian	Hawker Group	H	No	Massive, gray, well-indurated micritic limestone, in beds 2–3 meters thick. No larger grains or internal structure visible, aside from occasional irregular laminae.	Low-energy subtidal shelf deposition; gravitational settling	6H
		G	No	Weathered, poorly outcropping white sandy limestone	Not well exposed; likely transitional between shallow and shelfal marine	6G
Ediacaran	Rawnsley/ Bonney	F	No	Cross-stratified and planar- to irregularly laminated clean, mud-free quartz sandstone, in decimeter- to half-meter-scale beds. Individual beds may be indistinct. Tepee/petee structures (Gehling 1982) are seen occasionally, as well as small mud rip-up clasts on some bedding surfaces.	Shallow marine wave and current processes; possibly intertidal	6F, 7I
	Bonney Sandstone	E	Yes	Interbedded red shale, fine-grained sandstone, and pebble conglomerates. Conglomerates occur as decimeter-scale discrete beds, sometimes directly lying atop rippled surfaces with little apparent scouring or erosion. Sands and conglomerates may be parts of sandier intervals that fine upward. Sands in close association with conglomerates often contain high concentrations of heavy minerals, especially nearest to the diapir contact. Mudstones containing isolated clasts are also common. Max. clast size rarely exceeds small cobbles, except for immediately adjacent to the diapir where boulders occur. Clasts are of similar composition to, or of the same composition as Facies C below.	Paralic environments; fluvial, intertidal and marginal marine processes; intermittent gravity flows	6E, 7C–H
		D	No	Interbedded brick-red shales and fine-grained sandstones. Sands range from very common, centimeter-scale beds, to thicker decimeter- and half-meter-thick beds with planar and ripple lamination and cross-stratification. Sands often topped by asymmetrical or symmetrical ripples that are commonly draped by a thin mud layer. Many ripples have cm-scale wavelengths and sub-cm-scale amplitudes, and are sometimes flat-topped.	Intertidal and marginal marine processes; paralic environments	6D
	Wonoka Formation	C	Yes	Interbedded calcareous shale, limestone, and clastic pebble conglomerates. Conglomerates occur as discontinuous beds tens of meters across, often lens-shaped or with clear channel forms and scoured bases. Clasts range from sand- to cobble-size, dominated by pebbles, and the clast density is highly variable, ranging from dense gravel concentrations to individual grains interspersed in a sandy limestone matrix. Conglomerates composed primarily of lithified clasts of fine-grained sediments.	Shallow marine, storm influenced with intermittent gravity flows	6C, 7A, B
		B	No	Interbedded yellow calcareous shale and resistant limestone, very similar to Facies A. Color difference in the shales is the main feature that distinguishes Facies A and B, although cleaner, resistant limestones are more abundant in Facies A. Most similar to units 4, 5 or the "distal facies" of unit 7 in the classification of Haines (1987) or the "middle limestone member" of Kernen et al. (2012).	Shallow marine, storm influenced	6B
		A	No	Red calcareous shale and resistant limestones interbedded at varying, irregular frequency. Shales are planar-laminated and lacking in sedimentary structures. Limestone beds are 10–80 cm thick and massive, or containing hummocky cross-stratification planar and asymmetric-ripple lamination, and discrete beds of intraformational flat-pebble conglomerate. Limestones contain no visible grains and are composed of micrite with some degree of recrystallization.	Shallow marine, storm influenced	6A

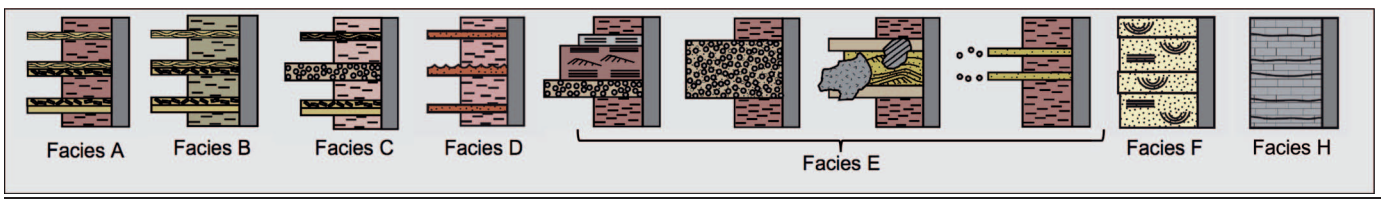

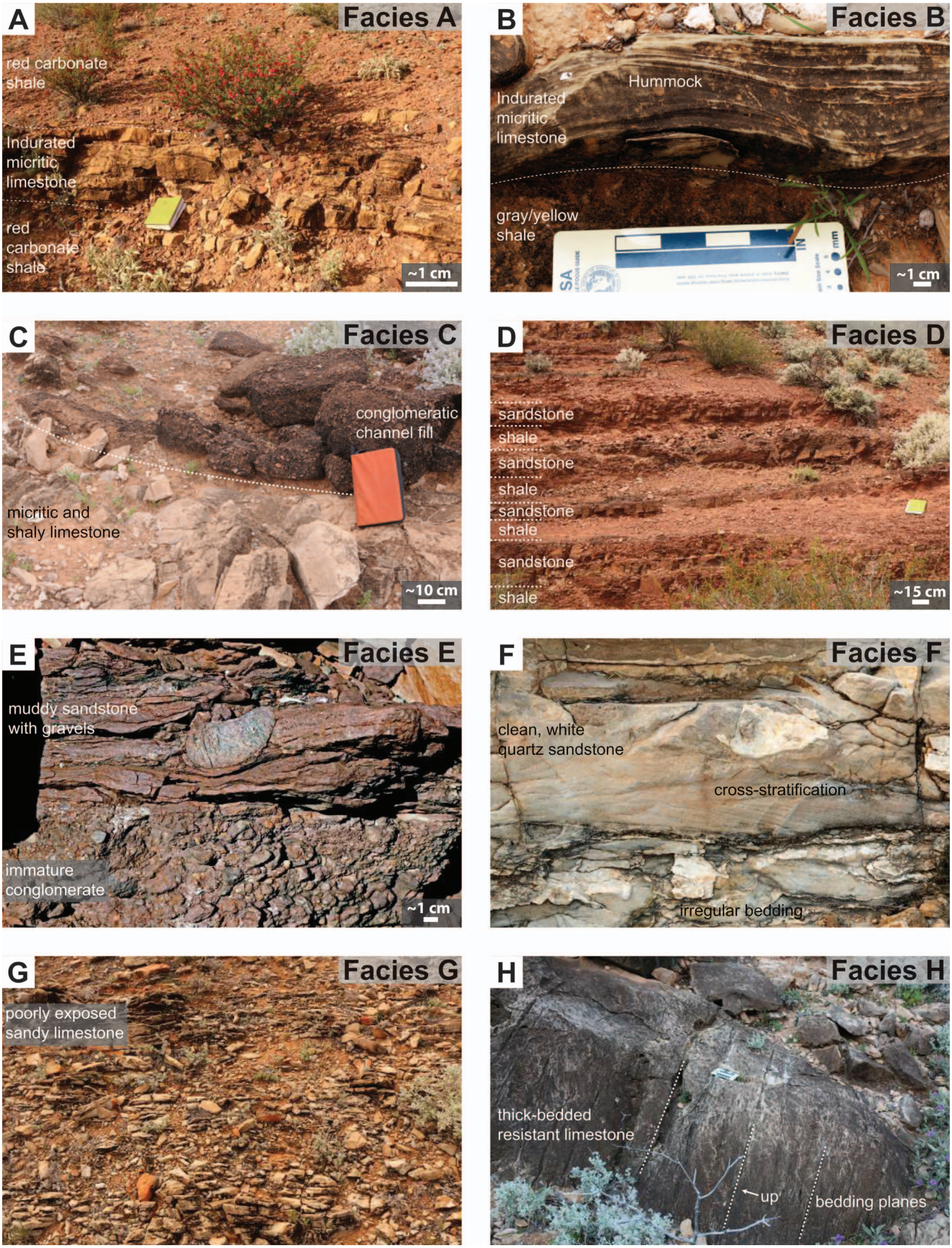

topographic high of the Mt. Frome diapir, where the exposed diapir matrix dissolved, leaving behind the insoluble clasts of the sediments interlayered with the original evaporites and brought upwards with the diapir. Clasts eroded downslope and were then reworked into adjacent deposits. Similar occurrences of redeposited diapir-derived sediments have also been seen in both continental and marine settings elsewhere, for example in the Cretaceous (Maastrichtian) of Spain (Hanisch and Pflug 1974), the Cretaceous–Tertiary of Mexico (Giles and Lawton 2002) and the Early Triassic of Utah (Lawton and Buck 2006). Discontinuous, massive, ungraded accumulations of pebbles in random orientations or with a faint horizontal fabric in a fine-grained matrix indicate that these deposits are the product of debris-flow processes (Ghibaudo 1992; Mulder and Alexander 2001). Given the surrounding shelfal context and the limestone matrix of the formation, these gravelly debrites were likely formed in a submarine environment. These deposits occur in beds that are laterally continuous for tens to hundreds of meters, or, less commonly, within channel forms having meter-scale widths, and are often overlain by carbonate-rich shales similar to those seen where extraformational conglomerates are absent. Channel forms indicate an earlier phase of erosive turbulent flow, with sediment bypass, as turbidite deposits are not preserved in the channels. Despite the wide range of clast sizes seen in the diapir, clasts within these conglomerate beds are all within a relatively narrow size range, indicating that they were hydrodynamically sorted before their deposition as debrites. While we interpret a submarine environment for these deposits, the diapir itself may have been subaerially exposed and formed an island, or may have been eroded subaqueously by wave and current action. Definitive evidence for either of these alternatives is not observed; however, the diapir must have been exposed in some form in order for clasts within it to be reworked into adjacent formations by sedimentary processes.

In Facies D and E, environments were significantly different. The switch to predominantly clastic deposition indicates a widespread change in sediment availability, and sedimentary features are indicative of different processes and settings. Gravel and sand beds (Fig. 8C–E) often have sharp bases and show evidence of incision, but discrete channel forms are rare. Ripple marks are common in sands throughout both of these facies, within and atop beds. Straight, symmetrical ripples with sub-centimeter-scale wavelengths and millimeter-scale amplitudes are evidence that water depth was very shallow (Immenhauser 2009), and current was oscillatory but weak. Differing crest orientations in closely adjacent beds (Fig. 8F), interference ripples (Fig. 8G), and thin mud drapes atop many ripple sets suggest changing current directions and depositional energies, potentially indicating tidal influence. Sand beds are also occasionally capped by flat-topped ripples (e.g., Fig. 8H), which form primarily when wave ripples are modified in very shallow water and during subaerial exposure (Tanner 1958; Reineck and Singh 1973). Although desiccation cracks are not seen, ripples at a similar scale with flat-topped geometries have been interpreted in the past as indicative of tidal-flat deposition (e.g., Tessier et al. 1995; Ericksson and Simpson 2012). Intervals where silty shales alternate with thin sands may thus have been deposited in a channelized, intertidal, marginal marine setting, such as a sand-dominated or mud-dominated tidal flat, with individual sand beds having been deposited in small channels, overbank splays, or washover fans (see Reading 1996).

Some intervals in Facies D and E appear to be more dominated by marine processes than others. Some sandy beds are normally graded (e.g., Fig. 8C), with increasing upward amounts of mud and ripple sets with progressively smaller wavelengths and amplitudes, indicating waning flow and decreasing depositional energy over the course of bed deposition. Such features are usually products of subaqueous gravity-flow deposition (e.g., Mulder and Alexander 2001; Talling et al. 2012). A marine interpretation is supported by the presence of thicker intervening packages of silty shales in some sections. These likely represent periods of low-energy, subtidal conditions, as the only other structures present are the occasional thin, sometimes fining-upward sand and gravel beds that may represent coarser material deposited farther offshore. Overall, Facies D is interpreted as shallow marine to paralic, an interpretation consistent with the general fluvial–deltaic setting of the formation throughout the larger basin (e.g., Gehling 1982; Counts et al. 2016).

Facies D and E are closely related. Aside from the presence of pebble-dominated conglomerates, background lithologies are very similar. Conglomerate clasts in Facies E (Fig. 8D, E) are of the same mixed composition as those in Facies C below—with the exception of intraformational flat limestone pebbles present in Facies C, Figure 8B—and also are interpreted to be sourced from the same exposed diapir material. As in the Wonoka Formation, grain sizes coarser than sand are generally not seen in the Bonney Sandstone outside of the immediate area surrounding diapirs (Counts 2016). Clasts similar to those observed here are present in the Bonney Sandstone adjacent to the nearby Pinda diapir (Hearon et al. 2015a). The paralic nature of Facies D suggests that the diapir body was likely at times exposed and eroded subaerially, though with marine environments nearby. Allochthonous salt carrying dense accumulations of clasts are also known to occur near subaerially (and subaqueously) exposed diapirs—these may also be subject to reworking by a variety of processes in the continental realm (e.g., Bruthans et al. 2009). Many pebble-bearing intervals of this facies are similar in character to alluvial-fan deposits, especially closest to the diapir in the more central measured sections (cf. Nilsen 1982). Some conglomerates in Facies E do have erosional bases, and may be reworked deposits that were deposited onto a tidal flat or shallow marine surface (as in Facies D) through small channels. On the northern and southern ends of the transect, where lithologies suggest more marine conditions, conglomerates are much less common. Those that are present may have been entrained within small

←

FIG. 7.—Example photographs of sedimentary facies seen in the study area. For full facies descriptions see Table 2. **A)** Facies A, showing two dominant lithologies of brick-red carbonate-rich shale and more resistant beds of gray-yellow micritic limestone. This facies similar to Facies B. **B)** Facies B, close-up of resistant limestone bed with HCS. Yellow carbonate-rich poorly exposed shales above and below. **C)** Facies C, showing scoured contact between gravel-filled channel and underlying shales and limestones. Base of channel marked by white line is in sharp contact with underlying limestones. **D)** Typical Facies D, in the Bonney Sandstone, showing alternating beds of brick-red fine sands and shales. **E)** Typical poorly sorted muddy conglomerates of Facies E. Conglomeratic beds often dominated by pebble-size clasts with a muddy, sandy matrix, with occasional larger cobbles. **F)** Quartz-dominated sandstones of Facies F, found in the Rawnsley Quartzite and certain parts of the upper Bonney Sandstone. **G)** Poorly exposed sandy limestones of Facies G. This facies is susceptible to weathering and does not crop out well throughout the study area. **H)** Massive, well-indurated limestones of Facies H.

→

FIG. 8.—Sedimentological features seen in Facies C, E, and F. **A**, **B)** Conglomerate layers in upper Wonoka Formation, Facies C, which often contain a mixture of rounded clastic pebbles and flat carbonate rip up clasts. **C)** Relatively complete Bouma sequence in Facies E, polished, slabbed hand sample; Bouma divisions annotated. **D)** Conglomeratic facies with abundant heavy-mineral laminae, Facies E. **E)** Facies E conglomerates, showing lithologic diversity of clasts in conglomerate intervals. **F)** Two sets of symmetrical ripples on adjacent bedding planes with paleocurrents 50–230° and 80–260°, Facies E, Section 4 (Fig. 4). **G)** Interference ripples atop sandstone bed affected by two or more current directions; Facies E, Section 5. **H)** Symmetrical flat-topped ripples with paleocurrents 105–285° in Facies E, Section 5 (Fig. 4); overlying rippled bed is a sandy pebble conglomerate marked by white dashed line. **I)** Petee structures in Facies F, similar to those described by Gehling (1982).

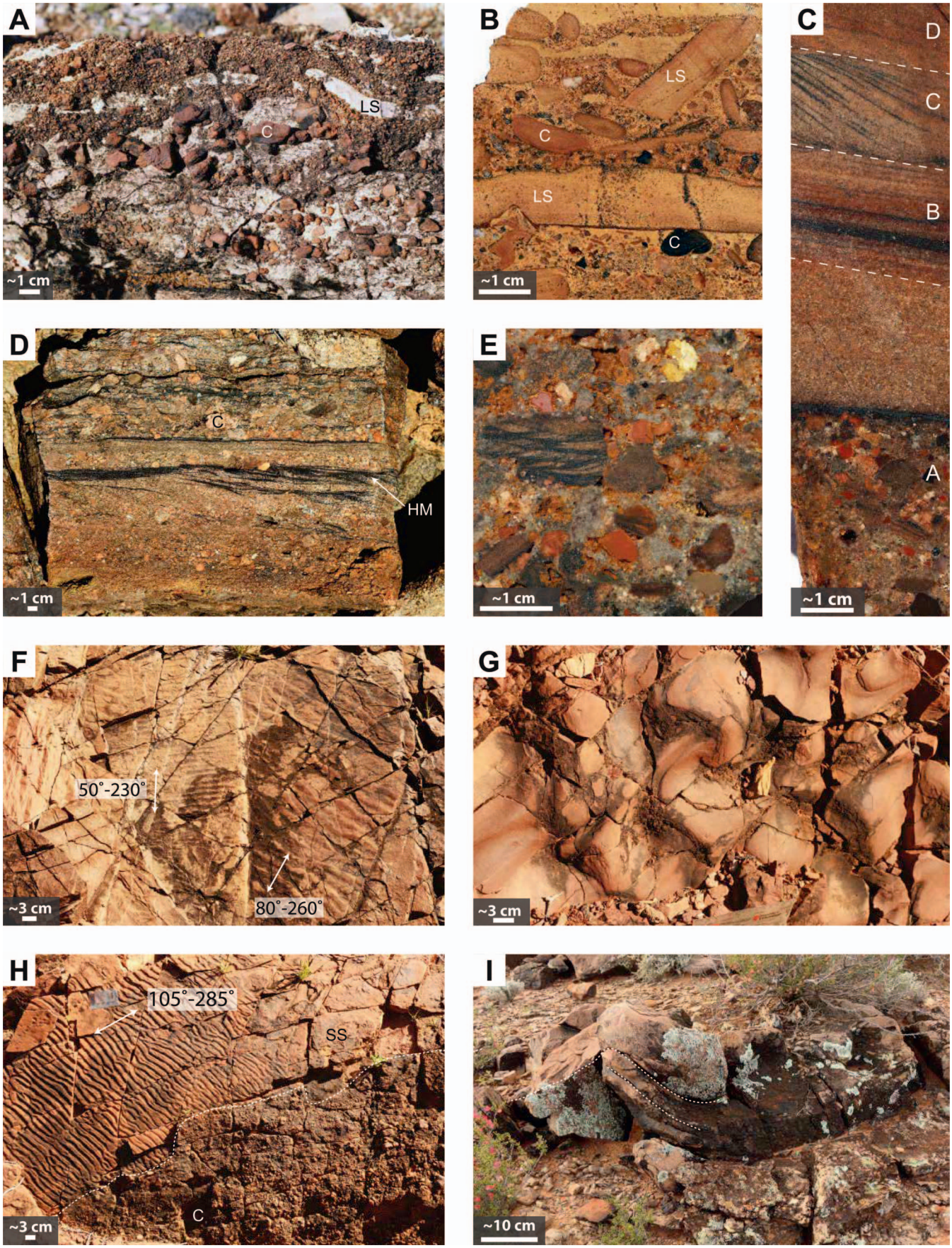

submarine sediment gravity flows and redeposited into the basin. Diapir-influenced sedimentation in Facies E may therefore take the form of direct deposition through debris-flow or sheetflood processes on proximal, subaerial alluvial fans (cf. Blair and McPherson 1994), downslope transport via fluvial processes, and further reworking through gravity, wave, and tidal processes in a shallow marine shoreface environment. This combination of multiple, variable processes affecting sediments within a relatively small area is not unprecedented; similar alluvial-fan–fluvial–shallow marine systems were described by Hayward (1985) in modern environments near the Red Sea, and Nemec and Steel (1984) noted several instances of transitional sequences where immature continental conglomerates interacted with marine processes when they reach the sea. Rather than being the product of an active tectonic setting, these types of interactions in Mt. Frome are a result of the local diapir-influenced environment in the area.

The quartzitic sandstones of Facies F may represent marine sediments deposited during a transgressive event. In the northern part of the section where this facies fills a large ($\sim$ 2 km) unit that erodes into the lower Bonney Sandstone, it may represent the marine fill of an incised valley. The white, well-sorted, cross-stratified sandstones do not show features associated with fluvial processes, such as fining-upward sequences and lateral-accretion surfaces. Beds are generally tabular, and sands are well-sorted, mature, and lacking in mud, characteristics generally not indicative of fluvial environments (Cant 1982). Where this facies occurs higher in the section (the upper parts of Sections 5–7; Fig. 6), it also contains irregular laminae that may be the result of algal binding. In this interval, sediments match previous descriptions of the Rawnsley Quartzite, which lies stratigraphically just below the well-known Ediacaran faunal assemblage (Gehling 2000). "Petee" structures (Fig. 8I) have also been cited as an intertidal indicator in these sediments, thought to be formed by expansive crystallization of evaporites in sands (Gehling 1982; 2000). This facies is thus interpreted as marine in origin.

Facies G is genetically more similar to the limestones above than the sandstones below, and likely represents the same shelf conditions as the remainder of the overlying Hawker Group. Its slightly higher clastic content, however, prevents crystallization and forming of resistant ledges. Neither Facies G nor the massive limestones of Facies H show diapiric influence, and are thus interpreted to have been deposited in an environment similar to that seen in the rest of the larger basin—a broad carbonate ramp of moderate depth with little depositional energy. Although archaeocyathid reefs are known from equivalent limestones in the area, they were not seen on the minibasin margin in the study area.

The distribution, character, and sequential stacking patterns of facies can be used to create qualitative depositional models that schematically reconstruct the Mt. Frome minibasin and diapir through time in a series of block diagrams (Fig. 9). These models show the changing influence of both the diapir itself and the overall background environmental conditions for each facies, as well as the distribution of hypothetical depositional elements in the minibasin.

DISCUSSION

Diapiric Influence on Sedimentary Character and Depositional Processes

Deposits in the Mt. Frome minibasin contain many sedimentary and stratigraphic features not seen in areas lacking in diapiric influence. The presence of these features here can best be explained by the proximity of the minibasin to a salt diapir that was intermittently exposed at the surface during times of deposition, either subaerially or on the seafloor, forming a topographic high. Abundant heavy mineral laminae, extraformational pebble and cobble conglomerates, and changes in overall stratigraphic architecture are all characteristic of some of the facies adjacent to the exposed Mt. Frome diapir. Clasts in gravity-flow deposits were lithified and incipiently reworked at the time of deposition, as evidenced by their roundness relative to those within the preserved diapir (compare Fig. 8E to Fig. 2B); these clasts are likely derived from the earliest basin fill sediments that were deposited along with evaporites.

In addition, strata in the minibasin can be characterized as having a substantial increase in the abundance of gravity flow deposits when compared to the same formations elsewhere in the region, resulting in a larger variety of deposit types than "background" sedimentation (e.g., discontinuous, heterolithic conglomerate beds are found only near diapirs). These deposits have a greater depositional energy than background sedimentation, and are in closer proximity to a source of large clasts. The discontinuous geometries and internal character of conglomeratic beds (massive to fining-upward) are consistent with deposition via subaerial and subaqueous sediment gravity flows (laminar and turbulent), which originated from the diapir and flowed into the minibasin depocenter. These deposits are most common nearest to the minibasin margin and where minibasin sediments thin onto the diapir near the central part of the transect. Destabilization and failure of the diapir on its margin, along with any overlying sediments, may be related to inflation and oversteepening of the diapir (Giles and Rowan 2012). Such failures and erosive events can be tied to halokinetic sequences, and the base of the Bonney Sandstone has been previously interpreted as a halokinetic sequence boundary in the nearby Patawarta diapir (Kernen et al. 2012).

Diapir-Related Controls on Facies Change

Although the current exposure of the minibasin margin is an oblique map view (Fig. 1C), the same units are laterally exposed for several kilometers, allowing the change in facies along the margin of the diapir to be observed. Stratigraphic units and the facies in them are variable in thickness and character along the minibasin margin, resulting in lateral heterogeneity of minibasin deposits. Lateral changes in facies are likely a result of the influence of structural features including faults, erosion, differential subsidence, and the rugosity and/or paleotopography of the diapir–sediment contact. Most notably, overall formation thicknesses below the Cambrian are considerably less near the middle of the transect between Sections 2 and 5 (Figs. 6, 8), and strata that are stratigraphically higher relative to the more northern and southern sections (sections 1 and 6–8) come in direct contact with the diapir. This change in thickness may be a result of a topographic high on the minibasin margin, or, alternatively, be a product of an oblique plane of exposure. Regardless, sediments in the Bonney Sandstone are in closer spatial and stratigraphic proximity to the diapir in these central sections, and sediments in this area contain a much higher abundance of conglomerates and other features that indicate sediment–diapir interaction. Sections seen on the north and south ends of the transect preserve additional units and facies not seen in the center, and contain facies more similar to "normal" background sediments (i.e., lacking in conglomerates).

The central part of the minibasin margin contains a number of features that may shed light on the increase in conglomerates in this area. In the study area, there are two primary fault complexes (shown with white arrows in Fig. 3B) that offset sediment to the south or southwest by tens of

→

FIG. 9.—Schematic block diagram reconstructions of depositional environments and local paleogeography in the Mt. Frome area over a series of time slices corresponding to each formation. Blocks are vertically exaggerated and not to scale. View of block diagrams is from obliquely south to north, roughly covering the area seen in Figure 3A. See labels and text for description of various elements.

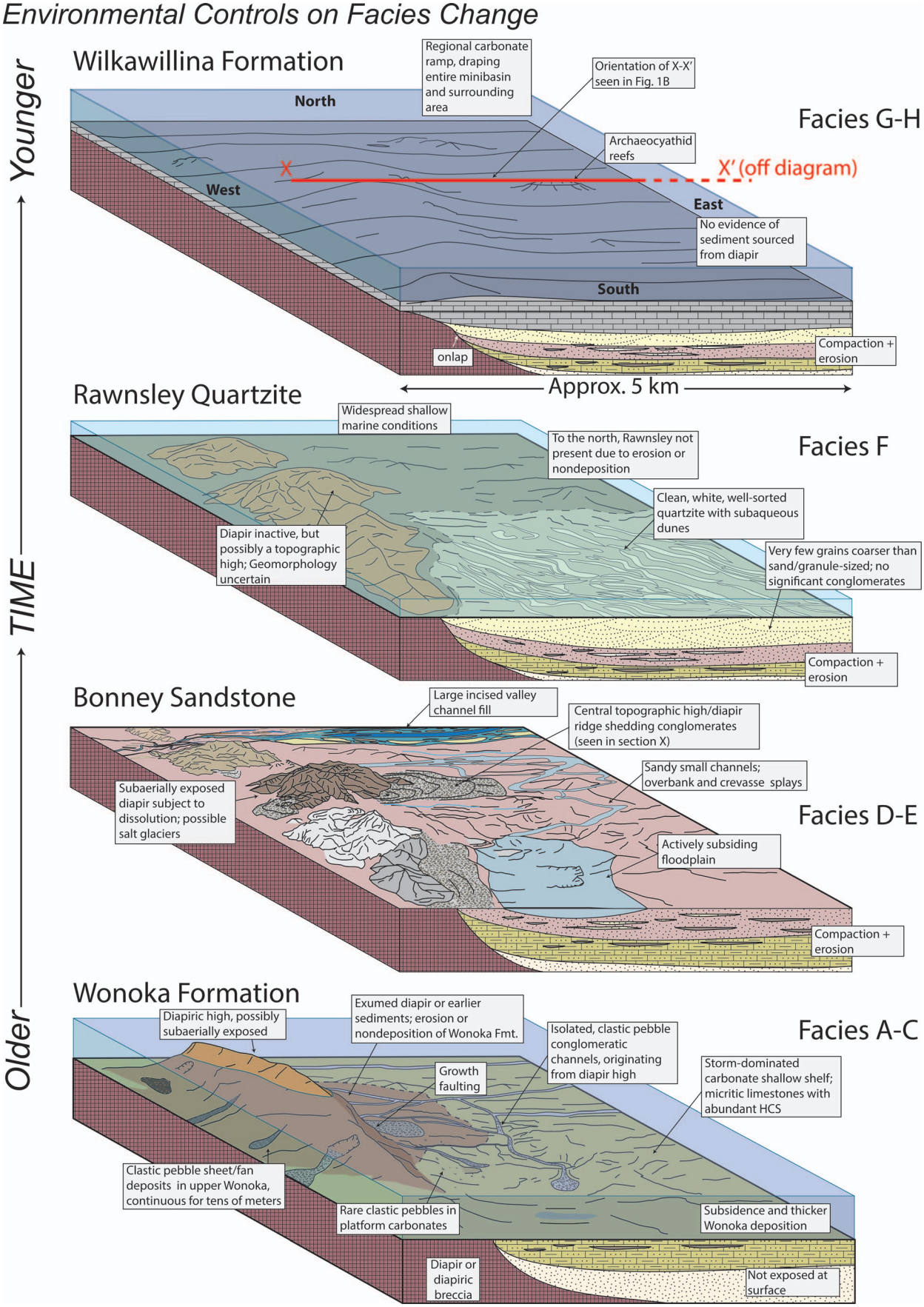

meters, laterally juxtaposing Facies D and E against the diapir body. The changes in sediment thickness across these faults indicate that they were likely syndepositionally active, but the sharp nature of some diapir–sediment contacts indicates that fault movement likely continued during early, pre-lithification burial. Brecciated and mineralized zones (Fig. 3B) adjacent to some faults also indicate post-burial movement. This brecciation, combined with abundance of smaller faults and lack of consistent exposure, generally prevents all but the largest individual beds from being traced across the fault. Correlation is also difficult as lithologies change laterally across faults; sediments seen in section 2, for instance, show a significant difference in the vertical distribution of sand and gravel beds compared to sections 2 and 3, which are on the downthrown side of faults. Growth faulting of sediment blocks between faults also caused them to be rotated, as evidenced by differing strike directions in the downthrown fault block near section 4 (Fig. 3B). It is possible that the diapiric "high" between Sections 3 and 4 may be caused by the accommodation of sediment at the toe of the northern growth fault. Similar geometries are seen in sandbox experiments done by Brun and Mauduit (2008, 2009), who modeled syndepositional fault growth atop a viscous medium that represents an underlying salt layer. This growth-fault-and-ridge geometry partially explains the overall geometry of the diapir margin. Such features are common components of models that describe the breakout and advance of allochthonous salt (e.g., Hudec and Jackson 2006). The diapir at Mt. Frome is interpreted as allochthonous as well (Rowan et al., in press), as it lies in between Wilpena Group strata (i.e., Wonoka and younger deposits in the minibasin discussed here, and the Brachina Formation to the southwest).

The occurrence of ridges and growth faults (labeled in Fig. 3B) is strongly correlative with the occurrence of conglomeratic Facies E, indicating that faulting and associated structural features control some aspects of facies distribution along the diapir margin. Fault scarps exposed newly eroded diapiric material and provided a source of coarser-grained sediment, which was then reworked and deposited through gravity-driven, mass-flow processes. Clasts from the diapir were rounded and redeposited into the discontinuous channels and lenses often seen in Facies C and E. Near the center of the transect where faulting is present and the diapir margin is more irregular, sedimentary units are thinner and background sedimentation rates are lower, and conglomerates thus form a higher proportion of the overall formation thickness (Fig. 6). Syndepositional faults and diapir proximity therefore affect facies stacking patterns along the minibasin rim across a kilometer-scale area, and are both associated with an increase in episodically deposited, diapir-derived conglomeratic lithologies. These conglomerates may be preferentially deposited in localized depocenters created by faults. Facies distribution also likely changes basinward, as the largest clast sizes are found closest to the diapir contact, and most often become smaller with increasing stratigraphic and spatial distance from the diapir.

Facies distribution in the Mt. Frome minibasin is therefore an interplay between the available accommodation, overall depositional environment, sediment source, diapir proximity and exposure, and sedimentation rates. An improved understanding of all of these factors can lead to improved models of the spatial distribution and stacking patterns of facies, including the net-to-gross ratio of conglomerates to sandy shales. While a facies model approach may prove beneficial to predicting facies distribution in minibasins, it may be equally useful to focus on understanding the depositional processes and controls on sedimentation in areas where salt and sediment interact at the surface.

Comparison with Diapir–Sediment Interaction Elsewhere

Similar sedimentologic features (and by extension, depositional processes) to those seen here have been recorded near other diapirs elsewhere, both in the Adelaide Rift Complex (e.g., Dalgarno and Johnson 1968; Dyson 1999; Lemon 2000; Dyson 2004a; Hearon et al. 2015a) and in other salt-influenced basins where salt is exposed at the surface (Giles and Lawton 2002). Elsewhere in the ARC, these include, but are not limited to:

- anomalously shallow-water deposits in otherwise deeper basins;
- rapid depositional process transitions over a small spatial area
- mixed clastic–carbonate lithologies;
- growth faulting both laterally and downdip from diapir margin that affects sediment thickness;
- angular unconformities associated with tilting; halokinetic sequences
- debris flows and turbidites resulting from diapir topography;
- paleocurrents that do not fit with larger basin paleogeography;
- condensed sedimentation on diapir margin;
- isolated exotic blocks and pebbles (diapir-derived detritus) in otherwise fine-grained strata.

Deposits near the Patawarta and Pinda diapirs ($\sim$ 50 km away) contain similar conglomeratic facies in the some of the same formations (i.e., in the Wonoka Formation at Patawarta, and the Bonney Sandstone at Pinda, although not in exactly the same stratigraphic intervals; see Table 2) as those seen here (Kernen et al. 2012; Hearon et al. 2015a), In these localities, evidence also suggests that salt breccias flowed laterally as allochthonous sheets or tongues into the surrounding sediments (Dyson 2004a; Hearon et al. 2015a). The presence of diapir-derived clasts is likely an indicator of diapir exposure; the occurrence of these clasts at approximately (though not exactly) the same stratigraphic intervals suggests that diapirs in multiple locations in the basin were exposed, and perhaps inflating, during approximately the same time frames. Hearon et al. (2015a) note that exposure of the Pinda diapir during Wilpena Group time was likely brief, as conglomeratic intervals are limited in extent both spatially and stratigraphically. Conglomerate deposits at Mt. Frome are also intermittently distributed, although specific exposure durations cannot be determined with certainty. Deposits in the Umberatana minibasin are also considered time-equivalent to the Bonney Sandstone (Counts and Amos 2016), and they contain large diapir-derived clasts and slump deposits, although the diapir body is not exposed nearby and direct relationships cannot be observed. These observations, combined with those reported here, confirm that a recurring pattern of characteristic sedimentary facies exist in these minibasin environments at specific stratigraphic intervals, and that such facies can be used to characterize diapir–sediment interaction in the basin on a general level. Taken individually, such features are not diagnostic of these settings, but they can be used as supporting evidence when direct relationships are not clear. Such features are likely to occur in other salt-tectonic provinces as well.

Active diapirs in present-day basins can be seen to break out onto a subaerial or subaqueous surface, providing a modern analogue for what may have occurred in the Mt. Frome area in the Precambrian. Emergent salt is seen today, for example, in and around the Persian Gulf, where diapirs sourced from Neoproterozoic evaporites (Edgell 1996) form salt glaciers (lacking a roof) on the surface (*namakiers;* Talbot and Pohjola 2009). Diapirs also occur offshore in that region, with circular salt bodies forming isolated, offshore islands on a shallow marine carbonate ramp with fringing coral reefs (Edgell 1996; Alsharhan and Kendall 2003; Peters et al. 2003; Thomas et al. 2015). Like the ancient diapirs described here, modern Arabian diapirs also contain abundant brecciated clasts brought to the surface from deeper in the basin, composed of widely varying lithologies and a wide range of sizes, up to kilometer scale. Insoluble clasts from exposed diapirs in Iran are reworked by fluvial processes (Bruthans et al. 2009), leading to deposits that may be superficially similar to the conglomerates seen here in Facies C and E. These instances provide some modern insight into the nature of minibasin deposits near Mt. Frome and

elsewhere in the Ikara–Flinders Ranges (and vice versa), and they are useful in understanding recurring features of these depositional settings. Many aspects of these types of deposits remain unknown from an actualistic perspective, however, and an opportunity exists for more work to be done that is focused on a better understanding of ancient salt-withdrawal minibasin fill.

Extrusive salt similar to that seen in Adelaide Rift Complex diapirs is observed in submarine settings as well, breaking out laterally along bedding planes (Wu et al. 1990) and forming open-toed allochthonous salt sheets that intersect the seafloor (Hudec and Jackson 2006). Subaqueous salt has been described in both ancient and modern sediments, for example, in Triassic strata in Tunisia (Masrouhi and Koyi 2012), and more recently in the Gulf of Mexico (Hudec and Jackson 2006), where salt breaks out from a thin sedimentary cover or forms subaqueous topographic highs in which the salt body is covered by a thin veneer of overlying sediment. The specific depositional processes and sedimentary characteristics operating near open-toed allochthonous salt on the seafloor have not been fully described in modern settings, where sedimentation is likely a complex interplay between salt movement and dissolution, reworking and redeposition of allochthonous clasts, and background sedimentation. Due to the difficulty of accessing such deposits on the seafloor, outcropping sediments in similar ancient settings provide the only insight into these processes. Mt Frome and other Ikara–Flinders Ranges diapirs may therefore provide the best opportunities to examine sedimentary processes and products in a setting analogous to that occurring today on salt-tectonized continental margins around the world.

CONCLUSIONS

Deposits in the Mt. Frome minibasin were deposited in a variety of shallow-marine and continental environments that were influenced by proximity to an extrusive diapir body. The exposure and uplift of the diapir body and the erosion of allochthonous clasts from within the diapir created a unique depositional setting and resulted in processes and products dissimilar to those found in the same formations elsewhere in the basin. Diapir-related features in the minibasin deposits include depositional thinning and onlap, rotational growth faulting, abundant pebble conglomerates (an anomalously large grain size for the interval) deposited in debrites and turbidites, and channelization. Conglomerates are sourced from growth-fault scarps that expose diapir matrix, leading to the deposition of diapir-derived pebble beds in lower shoreface, shallow marine, intertidal, and alluvial-fan environments. This study systematically describes the lateral variability of deposits along the rim of a salt-withdrawal minibasin, and is one of relatively few to study the detailed interaction of salt and sediment in an ancient setting from a sedimentological perspective. Both other diapirs in the region and modern diapirs elsewhere in the world show similar sedimentary facies in surrounding deposits; when combined with the observations reported here, this consistency shows that these settings contain a recurring set of features that can be useful in predicting the sedimentary character of these deposits. Such features can be used as sedimentological criteria for syndepositional salt movement and exposure when direct evidence is not present or more ambiguous, and can assist in creating predictive models of reservoir distribution in salt-influenced basins. This study further demonstrates that areas affected by salt tectonics should be considered unique sedimentary environments, as the processes operating and their resulting impact on sediments have no exact analogues elsewhere in the geologic record.

SUPPLEMENTAL MATERIAL

Locations of measured sections are available from JSR's Data Archive: https://www.sepm.org/pages.aspx?pageid=229.

ACKNOWLEDGMENTS

This work was supported primarily by the University of Adelaide International Postgraduate Research Scholarship and the AAPG Nancy Setzer Murray Memorial Grant. Additional support in the form of a postdoctoral fellowship and grant (ANR-10-LABX-19) provided by LabexMER. We thank Wirrealpa Station owners Barbara and Warren Fargher for property access, and we acknowledge the Adnyamathanha people, the traditional owners of the land on which this research is focused. Thanks to Sam Kobelt for assistance in the field. We also thank Dr. Thomas Hearon, Dr. Gregory Gordon, and JSR Associate Editor Dr. Jennifer Aschoff for helpful reviews and comments on this manuscript, which improved it greatly.

REFERENCES

Alsharhan, A.S., and Kendall, C.G.S.C., 2003, Holocene coastal carbonates and evaporites of the southern Arabian Gulf and their ancient analogues: Earth-Science Reviews, v. 61, p. 191–243.

Aschoff, J.L., and Giles, K.A., 2005, Salt diapir-influenced, shallow-marine sediment dispersal patterns: insights from outcrop analogs: American Association of Petroleum Geologists, Bulletin, v. 89, p. 447–469.

Backé, G., Baines, G., Giles, D., Preiss, W., and Alesci, A., 2010, Basin geometry and salt diapirs in the Flinders Ranges, South Australia: insights gained from geologically-constrained modelling of potential field data: Marine and Petroleum Geology, v. 27, p. 650–665.

Banham, S.G., and Mountney, N.P., 2013a, Evolution of fluvial systems in salt-walled mini-basins: a review and new insights: Sedimentary Geology, v. 296, p. 142–166.

Banham, S.G., and Mountney, N.P., 2013b, Controls on fluvial sedimentary architecture and sediment-fill state in salt-walled mini-basins: Triassic Moenkopi Formation, Salt Anticline Region, SE Utah, USA: Basin Research, v. 25, p. 709–737.

Banham, S.G., and Mountney, N.P., 2014, Climatic versus halokinetic control on sedimentation in a dryland fluvial succession: Sedimentology, v. 61, p. 570–608.

Blair, T.C., and McPherson, J.G., 1994, Alluvial fans and their natural distinction from rivers based on morphology, hydraulic processes, sedimentary processes, and facies assemblages: Journal of Sedimentary Research, v. 64, p. 450–489.

Bogdanova, S.V., Pisarevsky, S.A., and Li, Z.X., 2009, Assembly and breakup of Rodinia (some results of IGCP Project 440): Stratigraphy and Geological Correlation, v. 17, p. 259–274.

Booth, J.R., Dean, M.C., DuVernay, A.E., and Styzen, M.J., 2003, Paleo-bathymetric controls on the stratigraphic architecture and reservoir development of confined fans in the Auger Basin: central Gulf of Mexico slope: Marine and Petroleum Geology, v. 20, p. 563–586.

Brun, J.P., and Mauduit, T.P.O., 2008, Rollovers in salt tectonics: the inadequacy of the listric fault model: Tectonophysics, v. 457, p. 1–11.

Brun, J.P., and Mauduit, T.P.O., 2009, Salt rollers: structure and kinematics from analogue modelling: Marine and Petroleum Geology, v. 26, p. 249–258.

Bruthans, J., Filippi, M., Asadi, N., Zare, M., Šlechta, S., and Churáčková, Z., 2009, Surficial deposits on salt diapirs (Zagros Mountains and Persian Gulf Platform, Iran): characterization, evolution, erosion and the influence on landscape morphology: Geomorphology, v. 107, p. 195–209.

Bryant, W.R., Bryant, J.R., Feeley, M.H., and Simmons, G.R., 1990, Physiographic and bathymetric characteristics of the continental slope, northwest Gulf of Mexico: Geo-Marine Letters, v. 10, p. 182–199.

Cant, D.J., 1982, Fluvial facies models and their application, *in* Horn, M.K., ed., Sandstone Depositional Environments: American Association of Petroleum Geologists, Memoir 31, p. 115–137.

Cooper, A.M., 1991, Late Proterozoic hydrocarbon potential and its association with diapirism in Blinman #2, central Flinders Ranges, South Australia [Honours Thesis]: University of Adelaide, Australia, 48 p.

Counts, J.W., 2016, Sedimentology, Provenance, and Salt–Sediment Interaction in the Ediacaran Pound Subgroup, Flinders Ranges, South Australia [Ph.D. Thesis]: University of Adelaide, 297 p.

Counts, J.W., and Amos, K., 2016, Sedimentology, depositional environments and significance of an Ediacaran salt-withdrawal minibasin, Billy Springs Formation, Flinders Ranges, South Australia: Sedimentology, v. 63, p. 1084–1123.

Counts, J.W., Rarity, F., Amos, K., Ainsworth, R.B., Lane, T., Morón, S., Trainor, J., and Valenti, C., 2016, Sedimentologic interpretation of an Ediacaran delta: Bonney Sandstone, South Australia: Australian Journal of Earth Sciences, v. 63, p. 257–273.

Dalgarno, C.R.1964, Lower Cambrian stratigraphy of the Flinders Ranges: Royal Society of South Australia, Transactions, v. 88, p. 129–144.

Dalgarno, C.R., and Johnson, J.E., 1968, Diapiric structures and late Precambrian–early Cambrian sedimentation in Flinders Ranges, South Australia, *in* Braunstein, J., and O'Brien, G.D., eds., Diapirism and Diapirs: A Symposium: American Association of Petroleum Geologists, Memoir 8, p. 301–314.

Dyson, I.A., 1999, The Beltana Diapir: a salt withdrawal mini-basin in the northern Flinders Ranges: Mines and Energy of South Australia, Journal, v. 15, p. 40–46.

Dyson, I.A., 2004a, Christmas Tree Diapirs and Development of Hydrocarbon Reservoirs: A Model from the Adelaide Geosyncline, South Australia, *in* Post, P.J., Olson, D.L., Lyons, K.T., Palmes, S.L., Harrison, P.F., and Rosen, N.C., eds., Salt–Sediment Interactions and Hydrocarbon Prospectivity: Concepts, Applications, and Case Studies for the 21st Century: SEPM, Gulf Coast Section, 24th Annual Bob F. Perkins Research Conference, p. 133–165.

Dyson, I.A., 2004b, Geology of the eastern Willouran Ranges: evidence for earliest onset of salt tectonics in the Adelaide Geosyncline: Mines and Energy South Australia, Journal, v. 35, p. 48–56.

Edgell, H.S., 1996, Salt tectonism in the Persian Gulf basin, *in* Alsop, G.I., Blundell, D.J., and Davison, I., eds., Salt Tectonics: Geological Society of London, Special Publication 100, p. 129–151.

Ericksson, K.A., and Simpson E., 2012, Precambrian tidal facies, *in* Davis, R.A., and Dalrymple, R.W., eds., Principles of Tidal Sedimentology: The Netherlands, Springer, p. 397–419.

Gehling, J.G., 1982, Sedimentology and Stratigraphy of the Late Precambrian Pound Subgroup, Central Flinders Ranges, S.A. [MSc Thesis]: University of Adelaide, Australia, 111 p.

Gehling, J.G., 2000, Environmental interpretation and a sequence stratigraphic framework for the terminal Proterozoic Ediacara Member within the Rawnsley Quartzite, South Australia: Precambrian Research, v. 100, p. 65–95.

Ghibaudo, G., 1992, Subaqueous sediment gravity flow deposits: practical criteria for their field description and classification: Sedimentology, v. 39, p. 423–454.

Giles, K.A., and Lawton, T.F., 2002, Halokinetic sequence stratigraphy adjacent to the El Papalote diapir, northeastern Mexico: American Association of Petroleum Geologists, Bulletin, v. 86, p. 823–840.

Giles, K.A., and Rowan, M.G., 2012, Concepts in halokinetic-sequence deformation and stratigraphy, *in* Alsop, G.I., Archer, S.G., Hartley, A.J., Grant, N.T., and Hodgkinson, R., eds., Salt Tectonics, Sediments, and Prospectivity: Geological Society of London, Special Publication 363, p. 7–31.

Haines, P.W., 1987, Carbonate shelf and basin sedimentation, late Proterozoic Wonoka Formation, South Australia [Ph.D. Thesis]: University of Adelaide, 152 p.

Haines, P.W., 1988, Storm-dominated mixed carbonate/siliciclastic shelf sequence displaying cycles of hummocky cross-stratification, late Proterozoic Wonoka Formation, South Australia: Sedimentary Geology, v. 58, p. 237–254.

Haines, P.W., 1990, A late Proterozoic storm-dominated carbonate shelf sequence: the Wonoka Formation in the central and southern Flinders Ranges, South Australia, *in* Jago, J.B., and Moore, P.S., eds., The Evolution of a Late Precambrian–Early Palaeozoic Rift Complex: The Adelaide Geosyncline: Geological Society of Australia, Special Publication 16, p. 177–198.

Hanisch, J., and Pflug, R., 1974, The interstratified breccias and conglomerates in the Cretaceous Flysch of the northern Basque Pyrenees: submarine outflow of diapiric mass: Sedimentary Geology, v. 12, p. 287–296.

Hayward, A.B., 1985, Coastal alluvial fans (fan deltas) of the Gulf of Aqaba (Gulf of Eilat), Red Sea: Sedimentary Geology, v. 43, p. 241–260.

Hearon, T.E., Rowan, M.G., Giles, K.A., Kernen, R.A., Gannaway, C.E., Lawton, T.F., and Fiduk, J.C., 2015a, Allochthonous salt initiation and advance in the northern Flinders and eastern Willouran ranges, South Australia: using outcrops to test subsurface-based models from the northern Gulf of Mexico: American Association of Petroleum Geologists, Bulletin, v. 99, p. 293–331.

Hearon, T.E., Rowan, M.G., Lawton, T.F., Hannah, P.T., and Giles, K.A., 2015b, Geology and tectonics of Neoproterozoic salt diapirs and salt sheets in the eastern Willouran Ranges, South Australia: Basin Research, v. 27, p. 183–207.

Hudec, M.R., and Jackson, M.P., 2006, Advance of allochthonous salt sheets in passive margins and orogens: American Association of Petroleum Geologists, Bulletin, v. 90, p. 1535–1564.

Hudec, M.R., and Jackson, M.P., 2007 Terra infirma: understanding salt tectonics: Earth-Science Reviews, v. 82, p. 1–28.

Immenhauser, A., 2009, Estimating palaeo-water depth from the physical rock record: Earth-Science Reviews, v. 96, p. 107–139.

James, N.P., and Gravestock, D.I., 1990, Lower Cambrian shelf and shelf margin buildups, Flinders Ranges, South Australia: Sedimentology, v. 37, p. 455–480.

Kernen, R.A., Giles, K.A., Rowan, M.G., Lawton, T.F., and Hearon, T.E., 2012, Depositional and halokinetic-sequence stratigraphy of the Neoproterozoic Wonoka Formation adjacent to Patawarta allochthonous salt sheet, Central Flinders Ranges, South Australia, *in* Alsop, G.I., Archer, S.G., Hartley, A.J., Grant, N.T., and Hodgkinson, R., eds., Salt Tectonics, Sediments, and Prospectivity: Geological Society of London, Special Publication 363, p. 81–105.

Knoll, A., Walter, M., Narbonne, G., and Christie-Blick, N., 2006, The Ediacaran Period: a new addition to the geologic time scale: Lethaia, v. 39, p. 13–30.

Lawton, T.F., and Buck, B.J., 2006, Implications of diapir-derived detritus and gypsic paleosols in Lower Triassic strata near the Castle Valley salt wall, Paradox Basin, Utah: Geology, v. 34, p. 885–888.

Leeson, B., 1970, Geology of the Beltana 1:63,360 map area: South Australia: Geological Survey, Report of Investigations, v. 35.

Lemon, N.M., 2000, A Neoproterozoic fringing stromatolite reef complex, Flinders Ranges, South Australia: Precambrian Research, v. 100, p. 109–120.

Li, Z.X., Bogdanova, S.V., Collins, A.S., Davidson, A., De Waele, B., Ernst, R.E., Fitzsimons, I.C.W., Fuck, R.A., Gladkochub, D.P., Jacobs, J., Karlstrom, K.E., Lu, S., Natapov, L.M., Pease, V., Pisarevsky, S.A., Thrane, K., and Vernikovsky, V., 2008, Assembly, configuration, and break-up history of Rodinia: a synthesis: Precambrian Research, v. 160, p. 179–210.

Masrouhi, A., and Koyi, H.A., 2012, Submarine "salt glacier" of Northern Tunisia, a case of Triassic salt mobility in North African Cretaceous passive margin, *in* Alsop, G.I., Archer, S.G., Hartley, A.J., Grant, N.T., and Hodgkinson, R., eds., Salt Tectonics, Sediments, and Prospectivity: Geological Society of London, Special Publication 363, p. 579–593.

Matthews, W.J., Hampson, G.J., Trudgill, B.D., and Underhill, J.R., 2007, Controls on fluviolacustrine reservoir distribution and architecture in passive salt-diapir provinces: insights from outcrop analogs: American Association of Petroleum Geologists, Bulletin, v. 91, p. 1367–1403.

Mawson, D., 1941, The Wilpena Pound formation and underlying Proterozoic sediments: Royal Society of South Australia, Transactions, v. 65, p. 295–300.

McKenzie, N., Jacquier, D., Isbell, R., and Brown, K., 2004, Australian Soils and Landscapes: An Illustrated Compendium: Melbourne, CSIRO Publishing.

Mulder, T., and Alexander, J., 2001, The physical character of subaqueous sedimentary density flows and their deposits: Sedimentology, v. 48, p. 269–299.

Nemec, W., and Steel, R., 1984, Alluvial and coastal conglomerates: their significant features and some comments on gravelly mass-flow deposits, *in* Koster, E.H., and Steel, R.J., eds., Sedimentology of Gravels and Conglomerates: Canadian Society of Petroleum Geologists, Memoir 10, p. 1–31.

Nilsen, T.H., 1982, Alluvial fan deposits, *in* Koster, E.H., and Steel, R.J., eds., Sedimentology of Gravels and Conglomerates: Canadian Society of Petroleum Geologists, Memoir 10, p. 49–86.

Paul, E., Flöttmann, T., and Sandiford, M., 1999, Structural geometry and controls on basement-involved deformation in the northern Flinders Ranges, Adelaide Fold Belt, South Australia: Australian Journal of Earth Sciences, v. 46, p. 343–354.

Peel, F.J., 2014, How do salt withdrawal minibasins form? Insights from forward modelling, and implications for hydrocarbon migration: Tectonophysics, v. 630, p. 222–235.

Peters, J.M., Filbrandt, J., Grotzinger, J., Newall, M., Shuster, M., and Al-Siyabi, H., 2003, Surface-piercing salt domes of interior north Oman, and their significance of the Ara Carbonate "Stinger" hydrocarbon play: Geoarabia, v. 8, p. 231–270.

Pilcher, R.S., Kilsdonk, B., and Trude, J., 2011, Primary basins and their boundaries in the deep-water northern Gulf of Mexico: origin, trap types, and petroleum system implications: American Association of Petroleum Geologists, Bulletin, v. 95, p. 219–240.

Plummer, P.S., 1978, The upper Brachina subgroup: a late Precambrian intertidal deltaic and sandflat sequence in the Flinders Ranges, South Australia [Ph.D. Thesis]: University of Adelaide, Australia, 170 p.

Posamentier, H.W., and Walker, R.G., 2006, Facies Models Revisited: SEPM, Special Publication 84, 532 p.

Preiss, W.V., 1987, The Adelaide Geosyncline: late Proterozoic stratigraphy, sedimentation, paleontology and tectonics: Geological Survey of South Australia, Bulletin, v. 53, 438 p.

Preiss, W.V., 1999, PARACHILNA, South Australia, sheet SH54-13, second edition: Geological Survey, 1:250,000 Series, Map and Explanatory Notes.

Preiss, W.V., 2000, The Adelaide Geosyncline of South Australia and its significance in Neoproterozoic continental reconstruction: Precambrian Research, v. 100, p. 21–63.

Preiss, W.V., Belperio, A.P., Cowley, W.M., and Rankin, L.R., 1993, Neoproterozoic, *in* Drexel, J.F., Preiss, W.V., and Parker, A.J., eds., The Geology of South Australia, Volume 1, The Precambrian: South Australian Geological Survey, Bulletin, v. 54, p. 170–203.

Reading, H.G., ed., 1996, Sedimentary Environments: Processes, Facies and Stratigraphy. Oxford, UK, Blackwell Publishing, 688 p.

Reid, P., and Preiss., W.V., 1999, Parachilna map sheet, South Australian Geological Survey: Geological Atlas, 1:250,000, 54-13.

Reilly, M.R.W., 2001, Deepwater Reservoir Analogue: Bunkers Sandstone, Donkey Bore Syncline, Flinders Ranges Australia [Honours Thesis]: University of Adelaide, Australia, 58 p.

Reineck, H.E., and Singh, I.B., 1973, Depositional Sedimentary Environments: with Reference to Terrigenous Clastics: Berlin, Springer-Verlag, 550 p.

Ribes, C., Kergaravat, C., Bonnel, C., Crumeyrolle, P., Callot, J.P., Poisson, A., Temiz, H., and Ringenbach, J.C., 2015, Fluvial sedimentation in a salt-controlled mini-basin: stratal patterns and facies assemblages, Sivas Basin, Turkey: Sedimentology, v. 62, p. 1513–1545.

Rowan, M.G., and Vendeville, B.C., 2006, Foldbelts with early salt withdrawal and diapirism: physical model and examples from the northern Gulf of Mexico and the Flinders Ranges, Australia: Marine and Petroleum Geology, v. 23, p. 871–891.

Rowan, M.G., Hearon, T.E., Kernan, R.A., Giles, K.A., Gannaway, C.E., Williams, N.J., Fiduk, J.C., Lawton, T.F., and Hannah, P.T., in press, A review of allochthonous salt tectonics in the Flinders and Willouran Ranges, South Australia: Australian Journal of Earth Sciences.

Talbot, C.J., and Pohjola, V., 2009, Subaerial salt extrusions in Iran as analogues of ice sheets, streams and glaciers: Earth-Science Reviews, v. 97, p. 155–183.

Talling, P.J., Masson, D.G., Sumner, E.J., and Malgesini, G., 2012, Subaqueous sediment density flows: depositional processes and deposit types: Sedimentology, v. 59, p. 1937–2003.

Tanner, W.F., 1958, An occurrence of flat-topped ripple marks: Journal of Sedimentary Petrology, v. 28, p. 95–96.

Tarhan, L.G., Planavsky, N.J., Wang, X., Bellefroid, E.J., Droser, M.L., and Gehling, J.G., 2017, The late-stage "ferruginization" of the Ediacara Member (Rawnsley Quartzite, South Australia): insights from uranium isotopes: Geobiology, v. 16, p. 1–14.

Tessier, B., Archer, A.W., Lanier, W., and Feldman, H.R., 1995, Comparison of ancient tidal rhythmites (Carboniferous of Kansas and Indiana, USA) with modern analogues, *in* Flemming, B.W., and Barthalonä, A., eds., Tidal Signatures in Modern and Ancient Sediments: International Association of Sedimentologists, Special Publication 24, p. 259–271.

Thomas, R.J., Ellison, R.A., Goodenough, K.M., Roberts, N.M., and Allen, P.A., 2015 Salt domes of the UAE and Oman: probing eastern Arabia: Precambrian Research, v. 256, p. 1–16.

Toniolo, H., Lamb, M., and Parker, G., 2006, Depositional turbidity currents in diapiric minibasins on the continental slope: formulation and theory: Journal of Sedimentary Research, v. 76, p. 783–797.

Wu, S., Bally, A.W., and Cramez, C., 1990, Allochthonous salt, structure and stratigraphy of the north-eastern Gulf of Mexico, Part II: Structure: Marine and Petroleum Geology, v. 7, p. 334–370.

Received 3 December 2017; accepted 31 October 2018.